J. Fluid Mech. (2010), *vol.* 646, *pp.* 327–338. © Cambridge University Press 2010
doi:10.1017/S0022112009993090

Contact in a viscous fluid. Part 1. A falling wedge

C. J. CAWTHORN[1] AND N. J. BALMFORTH[2,3]†

[1]DAMTP, Centre for Mathematical Sciences, Wilberforce Road, Cambridge CB3 0WA, UK

[2]Department of Mathematics, University of British Columbia, 1984 Mathematics Road, Vancouver, BC, V6T 1Z2, Canada

[3]Department of Earth and Ocean Science, University of British Columbia, 6339 Stores Road, Vancouver, BC, V6T 1Z4, Canada

(Received 14 March 2009; revised 28 October 2009; accepted 29 October 2009)

Computations are presented of the upward force on a two-dimensional wedge descending towards a plane surface due to the Stokes flow of an intervening viscous fluid. The predictions are compared with those of lubrication theory and an approximate analytical solution; all three predict a logarithmic divergence of the force with the minimum separation. An object falling vertically under gravity will therefore make contact with an underlying plane surface in finite time if roughened by asperities with sharp corners (with smooth surfaces, contact is made only after infinite time). Contact is still made in finite time if the roughened object also moves horizontally or rotates as it falls.

1. Introduction

Classical results in fluid mechanics suggest that a solid object falling under gravity through a viscous fluid should make contact with an underlying rigid surface only after an infinite time (Brenner 1961). This slow approach to contact results from the divergence of the lubrication pressure force stemming from the squeeze flow in the closing gap between the solid surfaces. While the result is straightforward to derive, it also seems a little unsatisfying in view of the intuition built from everyday experiences, which suggests that objects can touch in finite time, whether or not they are immersed in a fluid.

Finite-time contact has also recently been called upon to explain a number of related fluid mechanical phenomena, such as the fore-aft asymmetry of the paths of particles colliding in viscous fluid (Davis *et al.* 2003), the terminal velocities reached by particles rolling down inclined surfaces (Smart, Beimfohr & Leighton 1993) and the steady rolling of viscously lubricated, nested cylinders (Balmforth *et al.* 2007). In all these examples, asperities on the surfaces are required to make contact and hold the colliding objects apart by a roughly fixed distance, allowing fluid flow through the residual gap to provide drag. Although it has never been explicitly shown that true contact is necessary in this scenario, such behaviour is typically asserted.

Nevertheless, there are no obvious flaws in the theoretical prediction that contact occurs after infinite time. The simplest route to establishing the result is via Reynolds' (1886) lubrication theory, which applies to relatively smooth, slowly moving and nearly

† Email address for correspondence: njb@math.ubc.ca

https://doi.org/10.1017/S0022112009993090 Published online by Cambridge University Press

touching objects. A recent formal analysis (Gérard-Varet & Hillairet 2008) that does not adopt the usual approximations of lubrication theory (the Stokes approximation in conjunction with small aspect ratio) also demonstrates that objects with smooth surfaces cannot touch in finite time.

The purpose of the present work is to explore whether contact can occur in finite time when one adds some additional (and plausibly relevant) physical effects. More specifically, we discuss how the approach to contact is modified when one takes into account the presence of non-smooth asperities, the compressibility of the fluid or the elastic deformation of the solid surfaces. Asperities are the focus of this article, while compressibility and elasticity are explored by Balmforth, Cawthorn & Craster (2009); this article also summarizes the effect of slip and van der Waals forces. We couch both studies in two spatial dimensions, focusing presently on the descent of a wedge-shaped object. An alternative simple geometry would be an axisymmetrical cone, which arguably has greater physical realism. However, the wedge offers a more accessible geometry for the method with which we solve the flow problem (and, in particular, for our choice of boundary conditions).

The idea that asperities could affect contact is suggested by lubrication theory, which predicts that if the approaching surfaces are not locally smooth and flat, but sharper, then fluid flows more easily out of the intervening gap, weakening the divergence of the lubrication forces. Contact can then be approached in finite time (irrespective of whether the falling object is a wedge or a cone). Unfortunately, the geometry of the sharpened problem contradicts one of the underlying assumptions of lubrication theory (the characteristic horizontal scales must be much less than the vertical ones), calling into question the validity of that result. Here, we lift the key geometrical restrictions and solve the two-dimensional Stokes problem for the falling wedge (§ 2). Our main result is that the upward resistive force exerted on the descending wedge by the fluid scales logarithmically with the minimum gap thickness, as predicted by lubrication theory. Thus, the prediction that contact can be made in finite time is vindicated (at least for two-dimensional geometry; the corresponding result for a cone remains unproven, if plausible). We also illustrate how the situation changes when the corner of the wedge is smoothed out on a short spatial scale. Finally, we discuss in § 3 the application to sedimentation, including a consideration of whether the conclusions are changed when the wedge is allowed to move horizontally and rotate, as would happen in more realistic physical situations.

2. The wedge

In order to investigate the effect of a sharp asperity on contact, we consider the model Stokes problem of a falling wedge illustrated in figure 1. This model problem encapsulates how a corner-shaped asperity modifies the squeeze flow beneath an object sedimenting towards a flat wall in the simplest possible geometrical setting. However, using a wedge also introduces a complication in that the forces on the upper surface are not finite, if the object is taken to flare outwards to infinity. On the other hand, were we to demand that the wedge end at a finite distance from its apex, we would need to add the detailed boundary conditions there. We avoid these issues by solving for the Stokes flow beneath an infinite wedge, and then computing the upward resistive force on the wedge because of the flow beneath a pre-defined central section.

The wedge is symmetric about $x = 0$ and is pitched at angle α to the horizontal; as shown in figure 1, we consider a central section of width $2L$. The wedge apex

https://doi.org/10.1017/S0022112009993090 Published online by Cambridge University Press

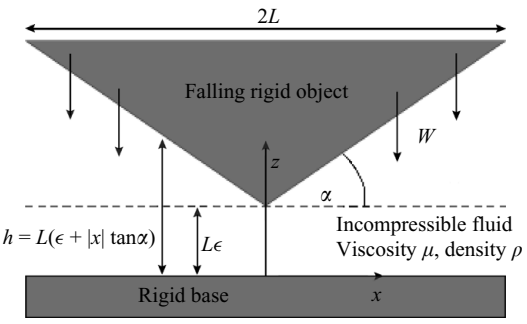


FIGURE 1. Diagram and notation for a vertically falling wedge.

lies at a distance $L\epsilon$ above the plane, and the wedge falls vertically. Motivated by gravitational settling, we cast the governing Stokes' equations into a dimensionless form by scaling lengths by L, velocities by $\sqrt{Lg}$, time with $\sqrt{L/g}$ and pressure with $\mu\sqrt{g/L}$, where g is the gravitational acceleration and μ is the fluid viscosity. The falling speed can then be written as $W = -\sqrt{Lg}\dot{\epsilon}$, and we arrive at the bi-harmonic problem for the (dimensionless) streamfunction, $\psi(x, z)$:

$$\nabla^4\psi = 0, \tag{2.1}$$

$$\psi(x, 0) = \psi_z(x, 0) = 0, \tag{2.2}$$

$$\psi_z(x, h(x)) = 0, \quad \psi_x(x, h(x)) = -\dot{\epsilon}, \tag{2.3}$$

$$\psi(0, z) = \psi_{xx}(0, z) = 0, \tag{2.4}$$

which incorporates the no-slip conditions on the lower and upper surfaces and the symmetry condition at $x = 0$ (the streamfunction is antisymmetric in x). The problem also demands far-field conditions to be placed on ψ for $|x| \to \infty$; these will be described below, after we derive an approximate solution. The velocity field, $(u, w) \equiv (\psi_z, -\psi_x)$, and the local thickness of the fluid layer is given by

$$h(x) = \epsilon + |x| \tan\alpha. \tag{2.5}$$

Using the solution to this problem, we will compute the upward force per unit width on the wedge from the section, $-1 \leqslant x \leqslant 1$:

$$F_z = -\int_{-1}^{1} \hat{\boldsymbol{z}} \cdot \begin{pmatrix} 2u_x - p & u_z + w_x \\ u_z + w_x & 2w_z - p \end{pmatrix}\bigg|_{z=h(x)} \cdot \begin{pmatrix} -\tan\alpha \\ 1 \end{pmatrix} \mathrm{d}x \tag{2.6}$$

$$= 2\int_0^1 \left[p - 2\frac{\partial w}{\partial z} + \left(\frac{\partial u}{\partial z} + \frac{\partial w}{\partial x} \right) \tan\alpha \right]_{z=h(x)} \mathrm{d}x, \tag{2.7}$$

where p is the (dimensionless) fluid pressure (which converges to an ambient pressure level far from the apex of the wedge that can be set to zero for our current problem).

2.1. *The approximate or outer solution*

If the wedge is relatively close to the lower plane (and so $\epsilon \ll 1$), an approximate solution follows on considering the corner flow illustrated in figure 2. The velocity boundary conditions on the solid surfaces correspond to those for the falling wedge. A simple analytical solution can be constructed for this configuration using polar coordinates (r, θ) centred at the corner itself (labelled O in the figure). In these

https://doi.org/10.1017/S0022112009993090 Published online by Cambridge University Press

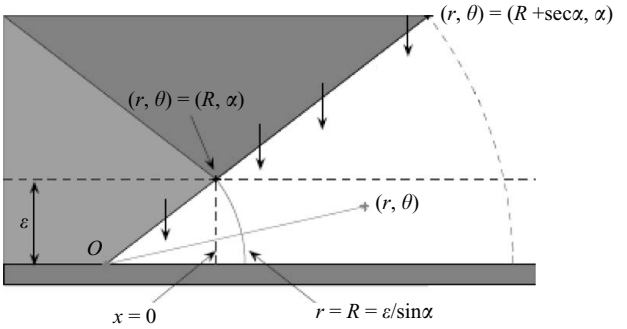


FIGURE 2. Diagram and notation for flow in a corner. The darker shaded region illustrates the wedge in figure 1, with symmetry axis $x = 0$.

coordinates, the streamfunction, $\psi(r, \theta)$, satisfies

$$\nabla^4 \psi = 0 \quad \text{in } 0 < \theta < \alpha, \tag{2.8}$$

$$\psi(r, 0) = \frac{\partial \psi}{\partial \theta}(r, 0) = 0, \tag{2.9}$$

$$\frac{\partial \psi}{\partial r}(r, \alpha) = -\dot{\epsilon} \cos \alpha, \quad \frac{\partial \psi}{\partial \theta}(r, \alpha) = r\dot{\epsilon} \sin \alpha, \tag{2.10}$$

with the radial and angular velocity components given by $U = r^{-1}\partial_\theta \psi$ and $V = -\partial_r \psi$, respectively.

A solution that satisfies these relations and corresponds to a bounded velocity field for $r \to \infty$ is given by

$$\psi(r, \theta) = \dot{\epsilon}[rg(\theta) + f(\theta)], \tag{2.11}$$

where

$$g(\theta) = -\frac{(\alpha + \sin \alpha \cos \alpha)(\theta \cos \theta - \sin \theta) + \theta \sin^2 \alpha \sin \theta}{\alpha^2 - \sin^2 \alpha} \tag{2.12}$$

and

$$f(\theta) = \frac{\epsilon \cos \alpha [(\cos 2\alpha - 1)(\cos 2\theta - 1) + \sin 2\alpha (\sin 2\theta - 2\theta)]}{4 \sin^2 \alpha (\sin \alpha - \alpha \cos \alpha)}. \tag{2.13}$$

Although (2.11) produces no net mass flux through $x = 0$ (or, equivalently, $r = R = \epsilon / \sin \alpha$), it does not satisfy the full symmetry conditions.

The approximation (2.11) also corresponds to the first two terms of a series solution with the separable form

$$\psi = \dot{\epsilon} \left[f(\theta) + rg(\theta) + \text{ Re} \left\{ \sum_{k=1}^{\infty} r^{2-\lambda_k} [A_k f_k(\theta) + B_k g_k(\theta)] \right\} \right], \tag{2.14}$$

where

$$f_k(\theta) = \frac{\cos[\lambda_k(\theta - \alpha/2)]}{\cos[\lambda_k \alpha/2]} - \frac{\cos[(\lambda_k - 2)(\theta - \alpha/2)]}{\cos[(\lambda_k - 2)\alpha/2]}, \quad \sin(\lambda_k - 1)\alpha = -(\lambda_k - 1) \sin \alpha, \tag{2.15}$$

https://doi.org/10.1017/S0022112009993090 Published online by Cambridge University Press

and

$$g_k(\theta) = \frac{\sin[\mu_k(\theta-\alpha/2)]}{\sin[\mu_k\alpha/2]} - \frac{\sin[(\mu_k-2)(\theta-\alpha/2)]}{\sin[(\mu_k-2)\alpha/2]}, \quad \sin(\mu_k-1)\alpha = (\mu_k-1)\sin\alpha \tag{2.16}$$

(cf. Moffatt 1964; Liu & Joseph 1977). The terms in the sum in (2.14) decay rapidly with r, implying that (2.11) provides a useful far-field approximation to the true streamfunction. Although the summed terms could also lead to a pattern of alternating eddies (Moffatt 1964), they are not apparent in any of the solutions we present later because they are dominated by the leading two terms, $f(\theta)+rg(\theta)$, which exhibit no such behaviour. In other words, we observe no infinite sequence of 'Moffatt' eddies here, unlike in several other problems involving Stokes flow in and around wedges.

The upward resistive force on the section of the upper surface, $R \leqslant r \leqslant R+\sec\alpha$ and $\theta=\alpha$, due to the corner flow, offers an approximation of $(1/2)F_z$:

$$F_z \approx F_O = -\dot{\epsilon}\left[\frac{2(2\alpha+\sin 2\alpha)}{(\alpha^2-\sin^2\alpha)}\log\left(1+\frac{\tan\alpha}{\epsilon}\right) - \frac{4\tan\alpha}{(\tan\alpha+\epsilon)(\tan\alpha-\alpha)}\right]. \tag{2.17}$$

For comparison, we quote the result expected from lubrication theory (see the Appendix):

$$F_z \approx F_L = \int_{-1}^{1} p\,\mathrm{d}x = -\frac{24\dot{\epsilon}}{\tan^3\alpha}\left[\log\left(1+\frac{\tan\alpha}{\epsilon}\right) - \frac{\tan\alpha}{2(\epsilon+\tan\alpha)}\right]. \tag{2.18}$$

Note that (2.17) reduces to (2.18) in the limit of a shallow wedge, $\alpha \ll 1$.

2.2. *The numerical solution*

The preceding arguments suggest that the approximate solution (2.11) provides the limiting far-field form for a full wedge solution. Thus, one can simplify numerical computations of that solution by truncating the domain at $x=\pm 1$ (which can be considered to lie in the far field when $\epsilon \ll 1$) and matching the streamfunction there to (2.11). Given this truncation, we numerically solve (2.1)–(2.5) by first mapping the region onto the unit square, via the transformation,

$$\xi = x, \quad \zeta = z/h(x). \tag{2.19}$$

It is then a simple matter to discretize the equations on a grid on the (ξ,ζ) plane by using a second-order finite-difference scheme, and turn the differential problem into an algebraic one. In order to resolve accurately the solution in the vicinity of the vertex of the wedge, we use a non-uniform grid distributed in a manner guided by the approximate solution.

Two sample solutions with different wedge angles are shown in figure 3. For smaller angles ($\alpha=\pi/12$ in figure 3), both the lubrication and outer solutions provide a good approximation for the horizontal velocity profile at $x=1$. However, the parabolic velocity profile predicted by lubrication theory does not match the computed solution for a sharper wedge ($\alpha=\pi/3$), because the aspect ratio is no longer small. Instead, the horizontal flux is concentrated towards the lower boundary, as predicted by the outer solution.

Plots of the vertical force as a function of ϵ are shown in figure 4. The force is a linear function of $\log\epsilon$ for small ϵ, with a pre-factor that is given by the approximate solution. At larger wedge angles, lubrication theory inaccurately estimates that pre-factor, leading to a force law with the wrong slope in figure 4(*a*).

https://doi.org/10.1017/S0022112009993090 Published online by Cambridge University Press

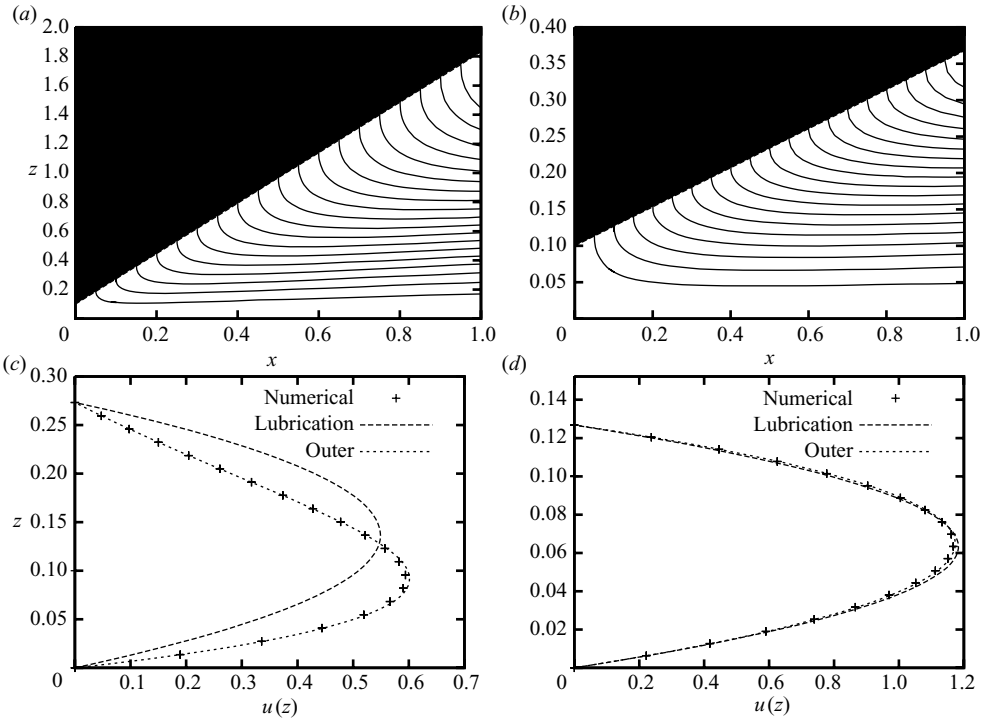


FIGURE 3. Stokes solutions with $\dot{\epsilon} = -1$ for wedges with $\epsilon = 0.1$ and $\alpha = \pi/3$ (*a,c*) or $\alpha = \pi/12$ (*b,d*). (*a,b*) Contour plots of the streamfunction on the (x, z) plane. (*c,d*) The horizontal velocity profile along the line $x = 0.1$, with predictions from the lubrication and outer solutions.

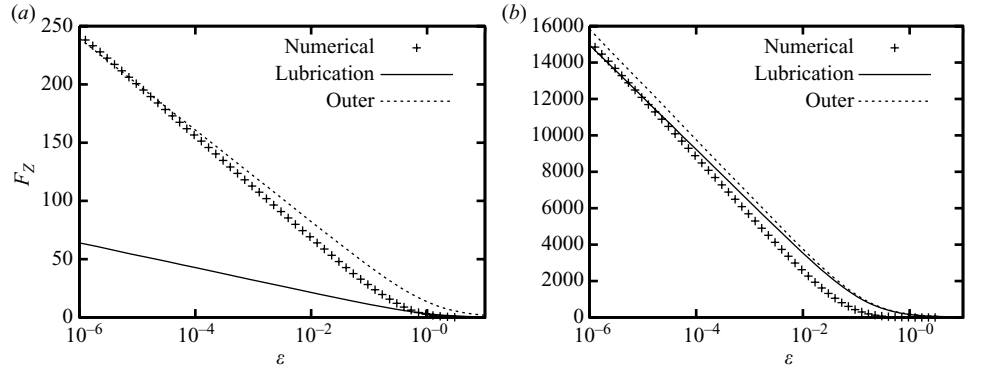


FIGURE 4. Plots of the vertical force F_z, with $\dot{\epsilon} = -1$, as determined by lubrication theory (2.18), the approximate Stokes solution (2.17) and the numerical solution, via (2.7), for wedges with angles (*a*) $\alpha = \pi/3$ and (*b*) $\alpha = \pi/12$.

2.3. *Smoothing out the corner at a smaller scale*

The argument that all physical surfaces are rough on some small length scale can readily be countered by an assertion that even a sharp asperity must be rounded on a yet smaller length scale. To illustrate the consequence of smoothing out the corner at a shorter scale, we carried out some further numerical computations for a rounded

https://doi.org/10.1017/S0022112009993090 Published online by Cambridge University Press

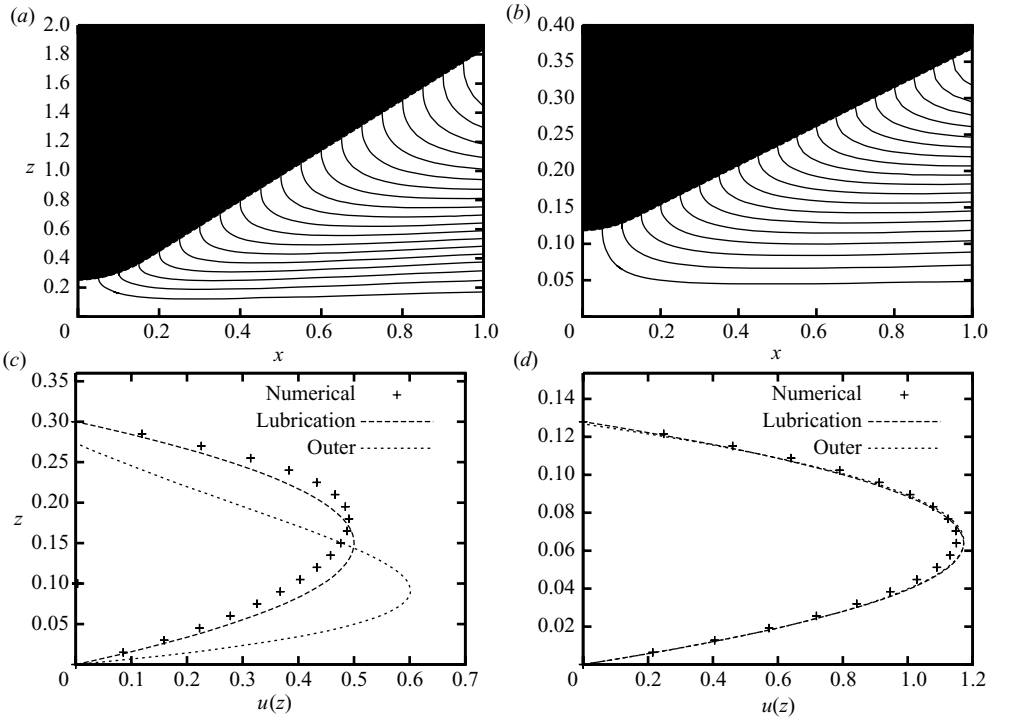


FIGURE 5. Stokes solutions with $\dot{\epsilon} = 1$ for rounded wedges with $\epsilon = 0.1$ and $(\alpha, \sigma) = (\pi/3, 0.1)$ (*a,c*) or $(\alpha, \sigma) = (\pi/12, 0.5)$ (*b,d*). (*a,b*) Contour plots of the streamfunction on the (x, z) plane. (*c,d*)The horizontal velocity profile along the line $x = 0.1$, with predictions from the lubrication and outer solutions.

wedge in which the fluid gap is given by

$$h(x) = \begin{cases} \epsilon + \dfrac{1}{2}\sigma \tan^2\alpha + \dfrac{1}{2}\sigma^{-1}x^2, & |x| < \sigma \tan\alpha, \\ \epsilon + |x| \tan\alpha, & |x| > \sigma \tan\alpha. \end{cases} \tag{2.20}$$

Sample numerical solutions, computed using the same scheme as described in § 2, are presented in figure 5. Away from the smoothed corner, the streamfunctions largely reproduce those computed for the full wedge; only for $x \sim \sigma \tan\alpha$ is there an appreciable difference.

The force on the rounded wedges is shown in figure 6, together with the approximation for the full wedge (2.17) and the leading-order lubrication result as the gap closes (cf. (A 5)),

$$F_{RL} = -3\sqrt{2}\pi\dot{\epsilon}\left(\frac{\sigma}{\delta}\right)^{3/2}, \tag{2.21}$$

where $\delta = \epsilon + (1/2)\sigma \tan^2\alpha$ is the actual minimum gap thickness. The full numerical solution converges to the lubrication prediction at the smallest separations; for larger gap thicknesses, the numerical result falls closer to the approximate solution for the full wedge. In other words, at the smallest separations, the lubrication pressure force reflects the smoothed corner, but at large separations the smoothing of the wedge is not felt and the descending object appears to have a real corner. The cross over

https://doi.org/10.1017/S0022112009993090 Published online by Cambridge University Press

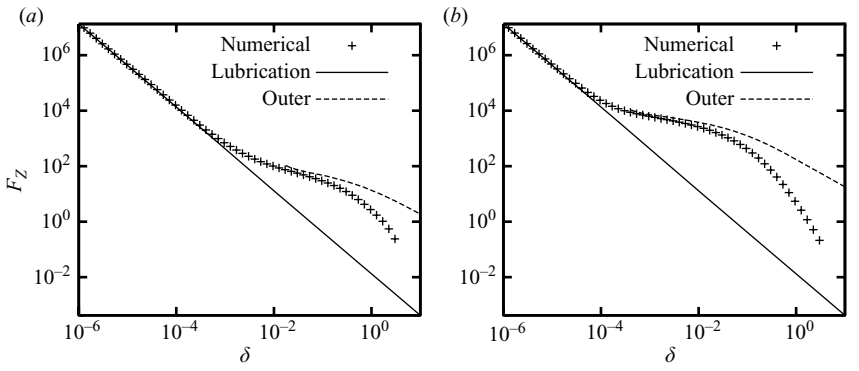


FIGURE 6. Plots of the vertical force F_z, with $\dot{\epsilon} = 1$, as determined by lubrication theory (2.21), the approximate Stokes solution (2.17) and the numerical solution, via (2.7), for rounded wedges with $\sigma = 0.01$ and limiting angles (*a*) $\alpha = \pi/3$ and (*b*) $\alpha = \pi/12$.

between the two regimes occurs for $\delta \sim \sigma \tan^2 \alpha$ (separations of the order of the radius of curvature of the rounded tip).

3. Sedimentation

3.1. *Vertical settling*

We now consider the dynamics of a wedge-shaped object falling under gravity. As mentioned earlier, however, the gravitational and hydrodynamic forces diverge for an infinitely wide wedge. We therefore shift focus and consider a finite wedge with our previous calculations describing the flow beneath its vertex and neglect any effect of the flow around the finite edges of the wedge.

We first consider purely vertical settling, with the left–right symmetry of the wedge ensuring that it does not tilt during the descent. The limiting form of the resistive force from the squeeze flow beneath the corner of the wedge indicates that, near contact, the equation of motion of the falling object reduces to

$$\mathscr{M}\frac{\mathrm{d}^2\epsilon}{\mathrm{d}t^2} \sim -1 - \nu(\alpha)\frac{\mathrm{d}\epsilon}{\mathrm{d}t}\log\frac{1}{\epsilon}, \tag{3.1}$$

where the dimensions of time have been chosen to scale gravitational accelerations to unity, $\nu(\alpha)$ is a constant, but angle-dependent, drag coefficient and $\mathscr{M}$ measures the inertia of the object. As we approach contact, the inertial term may be discarded, and we arrive at the key result

$$\epsilon \log\frac{1}{\epsilon} \sim \frac{(t_c - t)}{\nu(\alpha)}, \tag{3.2}$$

where t_c is a finite contact time.

For a wedge that is rounded at a small length scale, the logarithmic divergence of the drag force applies over an intermediate range of gap thickness, but ultimately switches back to the algebraic divergence expected for smooth surfaces. The switch occurs for separations that are of the same order as the smoothing scale. Thus, although contact no longer occurs in finite time, the sharpness of the asperity accelerates the initial approach to contact.

https://doi.org/10.1017/S0022112009993090 Published online by Cambridge University Press

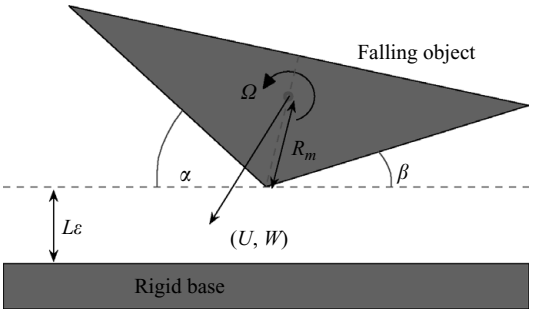


FIGURE 7. Diagram and notation for a falling, rotating and translating wedge.

3.2. *Settling with translation and rotation*

We now allow the wedge full freedom of movement so that it may tilt as it descends as a result of some initial asymmetric orientation, in order to determine whether this influences the approach to contact. One danger is that the wedge may tip over onto one side, falling with one face horizontal, significantly increasing the lubrication force and delaying contact. Alternatively, horizontal motion of a tilted wedge can generate lift, as in the classical Reynolds bearing. Thus, we need to check that the case of purely vertical settling is not overly idealized before we can conclude that contact occurs in finite time in generic situations. Note that the wedge will also necessarily tilt because of the torque induced by any left–right asymmetry.

The geometry of the problem is sketched in figure 7. The position of the wedge's apex is $(x_0(t), \epsilon(t))$, which can be related geometrically to the position of the centre of mass using the distance between those points, R_m, the opening angle of the wedge, $\pi - \alpha(t) - \beta(t)$, and the tipping angle, $\alpha(t) - \beta(t)$, as is evident in figure 7. The centre of mass of the wedge has velocity, $(U(t), W(t))$, and rotation rate, $\Omega(t)$; these can again be connected geometrically to $\mathrm{d}x_0/\mathrm{d}t$ and $\mathrm{d}\epsilon/\mathrm{d}t$. The problem now reduces to formulating the equations of motion of the wedge, which amount to ordinary differential equations for $(\epsilon(t), x_0(0), \alpha(t))$, once the forces and torque on the wedge are computed.

To ensure that the analysis remains tractible, we restrict attention to a wedge with a shallow opening angle, so that angles (α, β) remain small. We can then exploit the lubrication approximation, which, as demonstrated above, yields an adequate expression for the vertical hydrodynamic force. With this approximation, we can analytically compute the force on the wedge, (F_x, F_z), and the torque, G, about its apex. To $O(\alpha^2, \beta^2)$, these are given (dimensionlessly) by

$$F_x = \int_{-1}^{1} \left(-p \frac{\partial h}{\partial x} - \frac{\partial u}{\partial z} \right) \mathrm{d}x, \tag{3.3}$$

$$F_z = \int_{-1}^{1} p \, \mathrm{d}x, \tag{3.4}$$

$$G = \int_{-1}^{1} |x| p \, \mathrm{d}x, \tag{3.5}$$

where h is the thickness of the fluid-filled gap beneath the wedge,

$$h(x) \approx \begin{cases} \epsilon + (x - x_0)\alpha & \text{for } x > x_0, \\ \epsilon - (x - x_0)\beta & \text{for } x < x_0. \end{cases} \tag{3.6}$$

https://doi.org/10.1017/S0022112009993090 Published online by Cambridge University Press

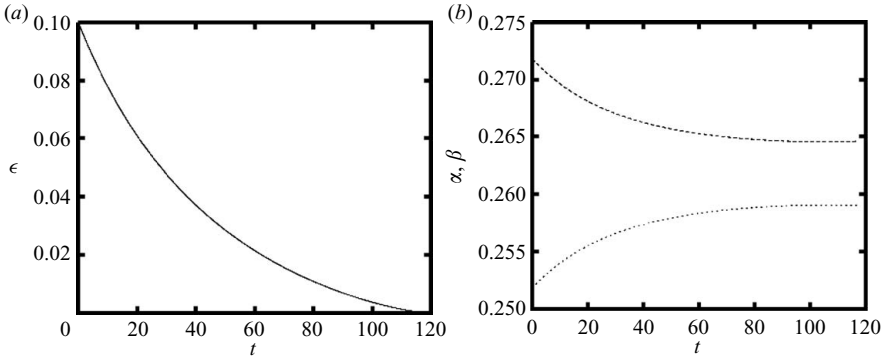


FIGURE 8. Numerical evolution of a sedimenting, tilting wedge, computed using lubrication theory. (*a*) The evolution of height ϵ and (*b*) the change in the angles (α, β). The computation begins from the initial conditions, $\epsilon(0) = 0.1$, $x_0(0) = 0$, $\alpha(0) = \pi/12 - 0.1$ and $\beta(0) = \pi/12 + 0.1$. Contact occurs in finite time near $t = 117$.

The pressure follows from integrating the lubrication equations along the lines outlined in the Appendix, albeit with the more general velocity boundary conditions for the translating and rotating wedge, and imposing $p = 0$ at the wedge's edges. Substitution of that result into the forces and torque leads to the relation

$$(F_x, F_z, G)^{\mathrm{T}} = \boldsymbol{A}(U, W, \Omega)^{\mathrm{T}}, \tag{3.7}$$

where the 'resistance matrix', $\boldsymbol{A}$, is quoted explicitly in the Appendix. Finally, for the eventual approach to contact, we neglect the wedge's inertia to arrive at the equations of motion of that object, which reflect force and torque balance:

$$F_x = 0, \tag{3.8}$$

$$F_z = 1, \tag{3.9}$$

$$G = R_m(\alpha - \beta)/2. \tag{3.10}$$

(Note that the horizontal displacement of the centre of mass from the apex of the wedge leads to a gravitational torque.)

To calculate the motion of the wedge, we first find and invert the matrix, $\boldsymbol{A}$, given the current geometry. Equation (3.7) then determines the velocity and the angular velocity of the centre of mass of the wedge. Geometrical relations connect these quantities to $(\dot{\epsilon}, \dot{x}_0, \dot{\alpha})$, providing the governing differential equations that we integrate numerically.

Figure 8 shows a sample, typical solution for a wedge beginning with a slight tilt, but no initial horizontal translation speed or rotation (indeed, without inertia, the initial velocity and rotation cannot be independently prescribed). A key feature is that the wedge still makes contact with the horizontal plane in finite time. Although the wedge does not right itself completely by the time of contact, the wedge tends to rotate in the direction that restores symmetry because the side of the wedge above the narrower fluid gap experiences a greater lubrication pressure than the opposite side. This pressure imbalance exerts a restoring torque that overcomes the gravitational torque and indicates that vertical descent is stable even towards relatively large perturbations (such motion can be shown to be stable towards infinitesimal perturbations using linear stability theory). Hence, we conclude that a wedge settling under gravity will,

https://doi.org/10.1017/S0022112009993090 Published online by Cambridge University Press

unless released with one face very nearly horizontal, make contact with a horizontal plane in finite time.

This work was initiated at the 2008 Geophysical Fluid Dynamics Summer Program, Woods Hole Oceanographic Institution, which is supported by the National Science Foundation and the Office of Naval Research. We thank the Program participants, R. V. Craster, L. Mahadevan and S. Llewellyn Smith for helpful discussions.

Appendix. Mathematical details

A.1. *Lubrication solution*

In lubrication theory, we reduce the dimensionless governing fluid equations for the velocity field (u, w) and pressure p to

$$p_x = u_{zz}, \quad p_z = 0, \quad u_x + w_z = 0. \tag{A 1}$$

Given that $u = 0$ on the two surfaces, we arrive at the Poiseuille velocity profile

$$u(x, z) = -\frac{1}{2} z(h - z) p_x. \tag{A 2}$$

Integrating the continuity equation across the gap, and imposing the conditions, $w(x, 0, t) = 0$ and $w(x, h, t) = -\dot{\epsilon}$, furnishes

$$-\dot{\epsilon} = \frac{\partial}{\partial x} \int_0^h u \, \mathrm{d}z = -\frac{1}{12} (h^3 p_x)_x, \tag{A 3}$$

from which it follows that

$$p = -\frac{6\dot{\epsilon}}{\tan^2 \alpha} \left(\frac{2}{h} - \frac{\epsilon}{h^2} \right), \tag{A 4}$$

satisfying $p \to 0$ as $x \to \infty$. The upward resistive force because of this pressure distribution from the region, $-1 \leqslant x \leqslant 1$, has been quoted in the text in (2.18).

Had the gap thickness been locally smooth, then $h(x) \approx \epsilon + x^2/2$. In this situation, the analogous result to (A 4) is $p = -6\dot{\epsilon}/h^2$, and the lubrication pressure force on the entire object (which is now integrable) is

$$\int_{-\infty}^{\infty} p \, \mathrm{d}x = -\frac{3\sqrt{2}\pi\dot{\epsilon}}{\epsilon^{3/2}}. \tag{A 5}$$

A.2. *Resistance matrix*

The coefficients of the resistance matrix $\boldsymbol{A}$ defined by (3.7) are given by

$$\left.\begin{aligned}
A_{11} &= 3\left(I_{02}^2 - \frac{4}{3} I_{01} I_{03}\right) \Big/ I_{03}, \\
A_{12} &= A_{21} = 6(I_{03} I_{12} - I_{13} I_{02})/I_{03}, \\
A_{13} &= A_{31} = 3(I_{03} I_{22} - I_{23} I_{02})/I_{03}, \\
A_{22} &= 12\big(I_{13}^2 - I_{03} I_{23}\big)/I_{03}, \\
A_{23} &= A_{32} = 6(I_{13} I_{23} - I_{03} I_{33})/I_{03}, \\
A_{33} &= \big(I_{23}^2 - I_{03} I_{43}\big)/I_{03},
\end{aligned}\right\} \tag{A 6}$$

where the integrals I_{mn} are defined by

$$I_{mn} = \int_{-L}^{L} \frac{x^m \, \mathrm{d}x}{[h(x)]^n}. \tag{A 7}$$

https://doi.org/10.1017/S0022112009993090 Published online by Cambridge University Press

REFERENCES

Balmforth, N. J., Bush, J. W. M., Vener, D. & Young, W. R. 2007 Dissipative descent: rocking and rolling down an incline. *J. Fluid Mech.* **590**, 295–318.

Balmforth, N. J., Cawthorn, C. J. & Craster, R. V. 2010 Contact in a viscous fluid. Part 2. A compressible fluid and an elastic solid. *J. Fluid Mech.* **646**, 339–361.

Brenner, H. 1961 The slow motion of a sphere through a viscous fluid towards a plane surface. *Chem. Engng Sci.* **16**, 242.

Davis, R. H., Zhao, Y., Galvin, K. P. & Wilson, H. J. 2003 Solid–solid contacts due to surface roughness and their effects on suspension behaviour. *Phil. Trans. Roy. Soc.: Math. Phys. Engng Sci.* **361**, 871–894.

Gérard-Varet, D. & Hillairet, M. 2008 Regularity issues in the problem of fluid–structure interaction. *Arch. Rat. Mech. Anal.*, doi:10.1007/s00205-008-0202-9.

Liu, C. H. & Joseph, D. D. 1977 Stokes flow in wedge-shaped trenches. *J. Fluid Mech.* **80**, 443–463.

Moffatt, H. K. 1964 Viscous and resistive eddies near a sharp corner. *J. Fluid Mech.* **18**, 1–18.

Reynolds, O. 1886 On the theory of lubrication and its application to Mr. Beauchamp Tower's experiments, including an experimental determination of the viscosity of olive oil. *Phil. Trans. Roy. Soc. Lond.* **177**, 157–234.

Smart, J. R., Beimfohr, S. & Leighton, D. T. 1993 Measurement of the translational and rotational velocities of a noncolloidal sphere rolling down a smooth inclined plane at low Reynolds number. *Phys. Fluids* A **5**, 13–24.

https://doi.org/10.1017/S0022112009993090 Published online by Cambridge University Press